

Czech Technical University in Prague
Faculty of Nuclear Sciences
and Physical Engineering

Department of Physics

Field: Physics and Technology of Thermonuclear Fusion



Vysoko-repetiční diagnostika
rentgenových impulzů generovaných
v laserovém plazmatu

High-repetition-rate diagnostics of
X-ray pulses generated in laser
plasma

RESEARCH PROJECT

Author: Bc. Michal Zhoř
Supervisor: Ing. Jaroslav Nejd, Ph.D.
Tutor: Dr. Dong-Du Mai, Dipl. Phys.
Year: 2020



Katedra: fyziky

Akademický rok:

2019/2020

VÝZKUMNÝ ÚKOL

Student: Bc. Michal Zhoř

Studijní program: Aplikace přírodních věd

Obor: Fyzika a technika termojaderné fúze

Vedoucí úkolu: Ing. Jaroslav Nejdrl, Ph.D. (FzÚ AV ČR),

konzultant Dr. Dong-Du Mai, Dipl. Phys. (FzÚ AV ČR)

Název úkolu (česky/anglicky): Vysoko-repetiční diagnostika rentgenových impulzů generovaných v laserovém plazmatu / High-repetition-rate diagnostics of X-ray pulses generated in laser plasma

Pokyny pro vypracování:

Navrhnete, sestavíte a otestujete systémy pro určení energetického spektra a počtu fotonů jednotlivých rentgenových impulzů generovaných v laserovém plazmatu, které je vytvořeno laserem s opakovací frekvencí 1 kHz.

- 1) Fyzikální principy určení spektra a počtu fotonů jediného rentgenového impulzu
- 2) Návrh zařízení schopných detekovat a zaznamenávat spektrum a počet emitovaných fotonů jednotlivých impulzů s opakovací frekvencí 1 kHz.
- 3) Sestavení a otestování zařízení.

Součástí zadání výzkumného úkolu je jeho uložení na webové stránky katedry fyziky.

Literatura:

- [1] D. Attwood, X-Rays and Extreme Ultraviolet Radiation: Principles and Applications, Cambridge University Press, Cambridge 2017.
- [2] J. Als-Nielsen, Elements of Modern X-ray Physics, 2nd Ed. Wiley 2011.
- [3] F. Zamponi et al. Femtosecond hard X-ray plasma sources with a kilohertz repetition rate, Appl. Phys. A 96 51 (2009).
- [4] P. Horowitz and W. Hill, The art of electronics, 3rd Ed., Cambridge University Press 2015.

Datum zadání: 25.10.2019

Datum odevzdání: 26.06.2020

vedoucí katedry

Prohlášení

Prohlašuji, že jsem svůj výzkumný úkol vypracoval samostatně a použil jsem pouze podklady (literaturu, projekty, SW atd.) uvedené v příloženém seznamu.

V Praze dne

.....
Bc. Michal Zhoř

Poděkování

Na tomto místě bych rád poděkoval Ing. Jaroslavu Nejdlovi, Ph.D. a Dr. Dong-Du Maiovi, Dipl. Phys. za příkladné vedení práce a podnětné rady.

Bc. Michal Zhoř

Název práce:

Vysoko-repetiční diagnostika rentgenových impulzů generovaných v laserovém plazmatu

Autor: Bc. Michal Zhoř

Studijní program: Application of Natural Sciences

Obor: Physics and Technology of Thermonuclear Fusion

Druh práce: Research project

Vedoucí práce: Ing. Jaroslav Nejdli, Ph.D.

Fyzikální ústav AV ČR, v.v.i.

Konzultant: Dr. Dong-Du Mai, Dipl. Phys.

Fyzikální ústav AV ČR, v.v.i.

Abstrakt: Práce nazvaná „Vysoko-repetiční diagnostika rentgenových impulzů generovaných v laserovém plazmatu“ studuje problematiku generace rentgenového záření v laserovém plazmatu a jeho diagnostiku. Výzkumný úkol se skládá z praktické a teoretické části. Teoretická část poskytuje nezbytné základy fyziky plazmatu a generace rentgenového záření, speciálně v laserovém plazmatu. Dále se zabývá detektory rentgenového záření a jejich potenciálním využitím pro plazmové rentgenové zdroje. Praktická část nejprve zkoumá diagnostiku rentgenového záření pomocí Braggovy difrakce, poté je představen koncept plazmového rentgenového zdroje v laserovém centru ELI Beamlines v Dolních Břežanech. V práci jsou popsány průběh a výsledky kontrolního měření pro uvedení do provozu. Hlavním úkolem je představit projekt plazmového rentgenového zdroje a přispět svým dílem k jeho výzkumu.

Klíčová slova: plasma, rentgenové záření, detektor, spektrum, laser

Title:

High-repetition-rate diagnostics of X-ray pulses generated in laser plasma

Author: Bc. Michal Zhoř

Abstract: The project titled "High-repetition-rate diagnostics of X-ray pulses generated in laser plasma" studies the topic of the X-ray generation in laser plasma and its diagnostics. The project comprises the theoretical and practical part. The theoretical part introduces the necessary plasma physics basics, the X-ray generation, especially in laser plasma. Moreover, it deals with the X-ray detectors with the potential of utilization in the field of plasma X-ray sources. The practical part includes the X-ray radiation diagnosis via Bragg diffraction as well as the design of the plasma X-ray source (PXS) in the laser facility ELI Beamlines. The process and results of commissioning are an essential part of the project too. The main goal is to introduce the PXS and contribute to its research.

Key words: plasma, X-ray radiation, detector, spectrum, laser

Contents

Symbols and Constants	8
Introduction	9
1 Plasma Physics	10
1.1 Propagation of Electromagnetic Waves through Plasma	11
1.1.1 Non-linear Phenomena	12
2 X-Ray Generation	14
2.1 Bremsstrahlung	14
2.2 Recombination	16
2.3 Characteristic Radiation	16
3 X-Ray Diagnostics and Detectors	18
3.1 X-ray Detectors	18
3.1.1 X-ray Film	18
3.1.2 PIN Diode	18
3.1.3 Phototube	19
3.1.4 Scintillator and Photomultiplier	20
3.1.5 Microchannel plate	20
3.1.6 Charge Coupled Device	21
3.1.7 Streak Camera	22
3.1.8 Geiger Tube	22
3.2 X-ray Spectral Characterisation	23
3.2.1 Bragg Diffraction	23
4 Plasma X-Ray Source	28
4.1 X-Ray Generation Principle	28
4.2 Scheme	28
4.2.1 Interior PXS layout	28
4.2.2 Beam Transport Chamber	30
4.2.3 Plasma Observation Unit	32
4.2.4 Laser Beam Profiler	33
4.2.5 X-Ray Core	33
4.2.6 X-Ray Shielding	35
4.3 Commissioning	35
4.3.1 Results	36

Summary	40
Bibliography	41

Symbols and Constants

Used symbols:

Symbol	Meaning
\mathbf{X}	Vector quantity X
X_i	i^{th} component of the vector quantity X
f	Scalar quantity f

Used constants¹:

Constant	Quantity	Value
c	Speed of light in vacuum	$c = 298,792,458 \text{ m}\cdot\text{s}^{-1}$
m_e	Invariant mass of an electron	$m_e \doteq 9.109,389 \cdot 10^{-31} \text{ kg}$
ε_0	Permittivity of vacuum	$\varepsilon_0 \doteq 8.854,187,817 \cdot 10^{-12} \text{ F}\cdot\text{m}^{-1}$
μ_0	Permeability of vacuum	$\mu_0 = 4\pi \cdot 10^{-7} \text{ N}\cdot\text{A}^{-2}$
h	Planck's constant	$h \doteq 4.135,699 \cdot 10^{-15} \text{ eV}\cdot\text{s}$
e	Electron charge	$e \doteq 1.602,177 \cdot 10^{-19} \text{ C}$

¹The constant values are taken from [3]

Introduction

The laser driven plasma X-ray sources are special X-ray sources which use laser-plasma interaction to generate high-energetic ultrashort radiation pulses of a duration in the order of femtoseconds. The development of these sources in the last decade provides a great opportunity to research structural dynamics of matter with high temperature or under high pressure [1]. The work focuses on the plasma X-ray source in ELI Beamlines laser facility. The laser beam has a repetition rate of 1 kHz and intended energy exceeding 100 mJ, even though the actual output pulse energy is only 20 mJ. The shot-to-shot variations create an urgent demand for accurate and reliable diagnostic tools in order to understand the involved processes properly.

In the first chapter, the project will outline basic plasma phenomena and their physical background. It is assumed that the mentioned phenomena could have an impact on the X-ray generation with the PXS. The chapter will provide essential view into the plasma physics and its attributes. In the next chapter, the X-ray generation will be described. There will be explained all significant mechanisms of the X-ray generation in the PXS², i. e. bremsstrahlung, recombination and characteristic radiation. The chapter is important for understanding the interactions among plasma particles leading to emitting an X-ray photon. The parts of PXS radiation spectrum will be examined. The third chapter will familiarize with the main X-ray detectors which are used in science and technology nowadays. Their advantages and disadvantages will be discussed as well as the suitability of their utilization. Finally, the practical part of the project will take place. The practical part will consist of two main sections. In the first part, the measurement of the X-ray tube spectra via Bragg diffraction will be described. The data acquired from the X-ray spectroscopy training in ELI Beamlines will be analysed and there will occur the efforts of the spectrum reconstruction. In the second part, the PXS itself will be described including its main systems and operation mode in detail. The results of the commissioning of the PXS will be introduced and the future steps will be outlined.

²but not only

Chapter 1

Plasma Physics

For understanding X-ray generation with the laser plasma, it is essential to know the physics of plasma generation. Plasma is commonly taken as the fourth state of matter. There are three properties of matter to be considered as plasma [2]:

- There are free carrier of charge (ions, electrons),¹
- Plasma shows a collective behavior,
- Plasma as a whole is neutral; it means that the charge of sufficient volume is roughly zero. It results from the shielding of the electric potential of one particle by the electric potential of the others on scales larger than Debye length².

Plasma is the most common state of matter in the universe. It naturally occurs e. g. in stars, nebulae and on Earth around lightnings [2]. Let us outline few parameters for describing plasma.

Cyclotron frequency and Larmor ratio

There are two important plasma parameters associated with magnetic induction \mathbf{B} , cyclotron frequency ω_c and Larmor ratio r_L . Charged particles in electromagnetic fields are under effects of Lorentz force

$$\mathbf{F} = Q(\mathbf{E} + \mathbf{v} \times \mathbf{B}), \quad (1.1)$$

where Q and \mathbf{v} are charge and velocity of particle, \mathbf{E} is an external electric field and \mathbf{B} is an external magnetic field. The outcome of solving the equation (1.1), especially the second member, is the oscillation of the charged particle in a circular trajectories around magnetic field lines with the frequency of ω_c , where

$$\omega_c = \frac{QB}{m}. \quad (1.2)$$

¹But it does not necessarily mean there are not any neutral particles in plasma.

²The concept of Debye length will be dealt later in this chapter.

The ratio of oscilation is called Larmor ratio and it is equal to

$$r_L = \frac{v_\perp}{\omega_c} = \frac{mv_\perp}{QB}, \quad (1.3)$$

where v_\perp is the magnitude of perpendicular component of the particle velocity.

Debye length

In vacuum, electrical potencial of free charged particle decrease like $\sim \frac{1}{r}$. In plasma, there is different relation caused with other charged particles screening out the potencial. This effect causes the decline of potencial like $\exp\left(-\frac{r}{\lambda_D}\right)$, where the characteristic length λ_D is exactly Debye length. The Debye length is closely connected to the plasmatic parameter N_D . The plasmatic parameter declares a number of particles in the volume with the radius of the Debye length. If $N_D \gg 1$, we talk about the ideal plasma where the colective behaviour dominates [2].

Plasma frequency

For studying plasma phenomena³, it is crucial to understand typical time and space scales. Talking about space, the Debye lenght or the Larmour radiuses are the significant values. The reciprocal expression for plasma frequency is considered to be the characteristic time of plasma waves and oscilations. Plasma frequency⁴ expresses the frequency of oscilations in the plasma caused by external electric field or internal disturbance of charge distribution, otherwise electrically neutral plasma in equilibrium. The Coulombic force is the force governing oscilations. For plasma frequency of particle α there is an expresion

$$\omega_{p\alpha} = \sqrt{\frac{n_\alpha Q_\alpha^2}{m_\alpha \varepsilon_0}}, \quad (1.4)$$

where n_α , Q_α , m_α are concentration⁵, charge and mass of particles α and ε_0 is the permittivity of vacuum [4].

1.1 Propagation of Electromagnetic Waves through Plasma

The electromagnetic waves (i.e. laser beam) cause many interesting phenomena while interacting with plasma [3]. The electromagnetic waves propagating through plasma

³Especially plasma waves and oscilations.

⁴Only electron plasma frequency can be taken into consideration because $\omega_p^2 = \omega_{pe}^2 + \omega_{pi}^2$ and $\omega_{p\alpha}^2 \sim m_\alpha^{-1}$ is valid, where ω_{pe} is electron plasma frequency, ω_{pi} is iont plasma frequency and $\alpha \in \{e, i\}$ [2].

⁵Strictly taken, it is concentration of undisturbed state.

affect mainly the electron part of plasma. The reason is that ions are too heavy for following high-frequency phenomena caused by electromagnetic waves. Assume external constant magnetic field \mathbf{B}_0 . The propagation of the electromagnetic waves through plasma will rely on the direction of the wave vector \mathbf{k} - there will be ordinary and extraordinary wave as well as it is in any crystals. Moreover, there will be two modes of the propagation in the parallel-to-magnetic-field direction: left-handed (L) and right-handed (R) electromagnetic waves⁶, see Fig. 1.1. R and L waves results from the dispersion relation for the electromagnetic waves. The direction right or left means the direction of the rotation of the plane of polarization caused by the component of magnetic field in direction of \mathbf{k} . The outcome is only the linear-approximated solution of the system of equation. The problem is rich in non-linear effects of the interaction, too [3].

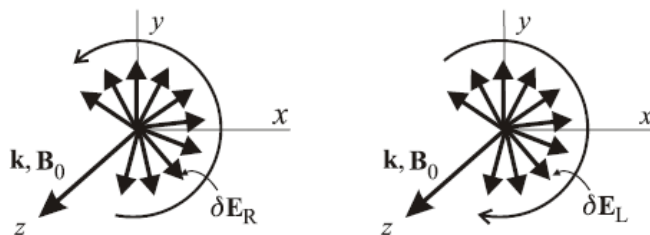


Fig. 1.1: Right-handed \mathbf{E}_R and left-handed \mathbf{E}_L electromagnetic waves [2].

1.1.1 Non-linear Phenomena

Non-linear phenomena in plasma are considered to be the phenomena which are consequent upon the non-linear term of plasma equations. There are many non-linear phenomena in plasma physics [3], i. e. Raman and Brillouin scattering, ponderomotive force, self-focusing of electromagnetic waves. In the following text, there will be described these ones which will be relevant for the project.

Ponderomotive Force

The electromagnetic waves exert a radiation pressure which is usually very weak. However, when high powered laser beams⁷ are used to heat or confine plasma, the radiation pressure can reach several hundred thousand atmospheres [5]. The force exerting the pressure is called ponderomotive force. Assume a wave electric field in the form

$$\mathbf{E} = \mathbf{E}_s(\mathbf{r})\cos(\omega t), \quad (1.5)$$

where \mathbf{E}_s is the spatial part of the electric field vector and ω is its frequency. A relation for the non-relativistic form of the ponderomotive force \mathbf{f}_p affecting one

⁶Left-handed (L) or right-handed (R) wave means that electric intensity vector \mathbf{E} changes its orientation to the left side or to the right side towards \mathbf{B}_0 , see Fig. 1.1.

⁷In the PXS, there is used laser beam with designed power $P \sim 5$ TW

particle with mass m and charge Q is, according to [5],

$$\mathbf{f}_P = -\frac{1}{4} \frac{Q^2}{m\omega^2} \nabla |\mathbf{E}_s|^2. \quad (1.6)$$

The relativistic generalisation⁸ is, according to [6], in the following form

$$\mathbf{f}_P = -mc^2 \nabla \sqrt{1 - \frac{Q^2 \langle \mathbf{E}_s \rangle^2}{m^2 \omega^2}} \quad (1.7)$$

Self-focusing

The phenomenon called self-focusing occurs for laser power $P_L > 2$ TW, [8]. Laser beam with actual parameters: output pulse energy 20 mJ and pulse duration 15 fs, but designed parameters are: output pulse energy 100 mJ and pulse duration < 20 fs, is utilized for the project. Actual power P_L almost reaches the threshold but the designed power P_L reaches it for sure. The relativistic disperse relation for the electromagnetic waves is taken for the derivation of mathematical background for self-focusing:

$$\omega^2 = c^2 k^2 + \frac{\omega_p^2}{\gamma}, \quad (1.8)$$

where γ is Lorentz factor. The corresponding refractive index $N(r)$ is

$$N(r) := \frac{ck}{\omega} = \left(1 - \frac{\omega_p^2}{\gamma \omega^2}\right)^{\frac{1}{2}}. \quad (1.9)$$

The ponderomotive force pushes electrons from the highest laser beam intensity causing the diminution of electron density. Therefore, the result is the decline of the plasma frequency which causes the growth of refractive index and then the focusing effect [8].

⁸A reader finds the derivation in [6]

Chapter 2

X-Ray Generation

In the following text, the work focuses on X-ray generation via free-free, free-bound and bound-bound mechanism. The free-free mechanism between free charged particles causes radiation called *bremsstrahlung*. The second process, recombination, is an interaction of free and bounded charged particles. The last mechanism are the transitions of electrons in electron shell causing an emission of photon. All three processes are depicted in Fig. 2.1. Particular components of the spectrum will be examined afterwards.

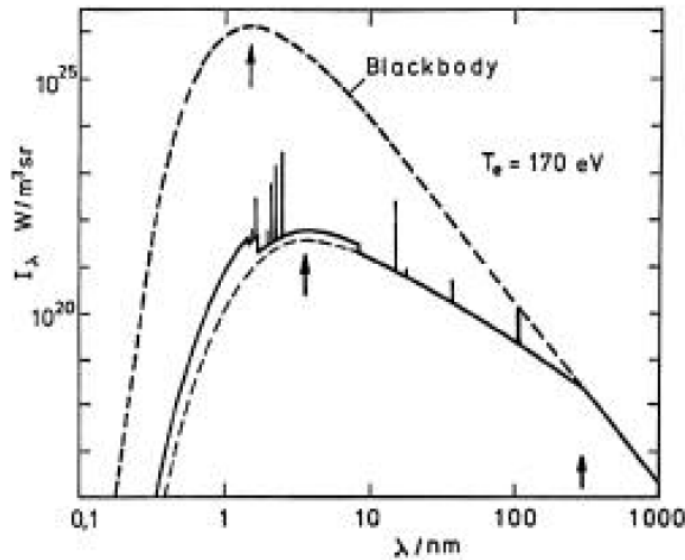


Fig. 2.1: Schematic radiation spectrum from a laser produced plasma compared to that of a blackbody at the same temperature [7].

2.1 Bremsstrahlung

The German word "Bremsstrahlung" is in English commonly used word for "braking radiation", i.e. radiation caused by accelerating¹ charged particles. Predominantly,

¹and decelerating

the bremsstrahlung occurs when an incident electron is accelerated as it passes a nucleus and causes the radiation [3]. The relation for the total radiated power of non-relativistic particle in direction $\mathbf{n} = \frac{\mathbf{R}}{R}$ is derivated from the Liénard-Wichert potentials, see Fig. 2.2. The whole derivation is complicated, therefore only the final part is shown in this work. An interested reader finds the complete derivation in [9]. An electric field \mathbf{E} is expressed as

$$\mathbf{E}(\mathbf{r}, t) = \frac{Ze}{4\pi\epsilon_0 c} \frac{\mathbf{n} \times (\mathbf{n} \times \dot{\beta}_0)}{R} \Big|_{t_0}, \quad (2.1)$$

where $\dot{\beta}_0 = \dot{\beta}_0(t_0) = \frac{\dot{\mathbf{v}}_0}{c}(t_0)$, $Ze = Q$ is a charge of particle and $t_0 = t - \frac{r}{c}$ is so called retarded time². A magnetic field \mathbf{H} is

$$\mathbf{H} = \frac{1}{Z_0} \mathbf{n} \times \mathbf{E}, \quad \text{where } Z_0 = \sqrt{\frac{\mu_0}{\epsilon_0}}. \quad (2.2)$$

The element of an energy flux dP through the element of an area $d\mathbf{f} = \mathbf{n}R^2d\Omega$ is

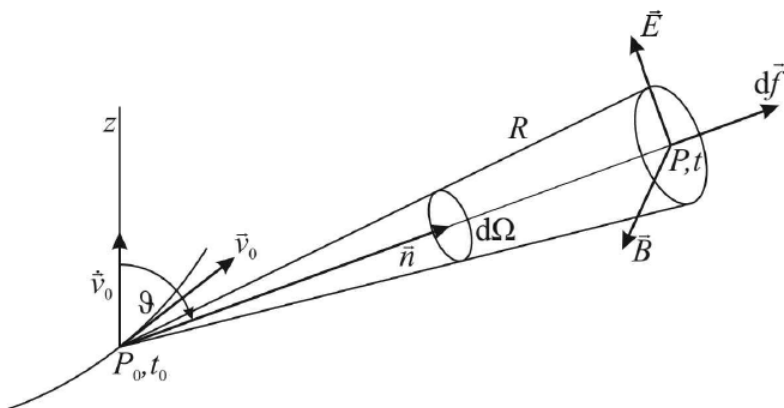


Fig. 2.2: The radiation of the charged particle to the solid angle $d\Omega$. Indices 0 denote the direct connection among the quantities and the particle [9].

expressed by the Poynting vector \mathbf{S} as

$$dP = \mathbf{S} d\mathbf{f} = (\mathbf{E} \times \mathbf{H}) \mathbf{n} R^2 d\Omega = \frac{1}{Z_0} \mathbf{E}^2 R^2 d\Omega. \quad (2.3)$$

Appointing (2.1) to (2.3) and regarding an identity

$$|\mathbf{n} \times (\mathbf{n} \times \dot{\mathbf{v}}_0)| = |\dot{\mathbf{v}}_0| \sin\vartheta, \quad (2.4)$$

where ϑ is an angle between $\dot{\mathbf{v}}_0$ and \mathbf{n} , it is derived angular distribution of radiated power

$$dP(t) = \frac{(Ze)^2}{(4\pi\epsilon_0 c^2)^2 Z_0} \dot{\mathbf{v}}_0(t_0)^2 \sin^2\vartheta d\Omega. \quad (2.5)$$

²Retarded time covers the time necessary for information to travel the distance between an observer and the charged particle.

By integrating over the full solid angle, the relation for the total radiated power is gained. It is commonly called Larmor relation:

$$P(t) = \frac{2}{3c^3} \frac{(Ze)^2}{4\pi\epsilon_0} \dot{\mathbf{v}}_0(t_0)^2. \quad (2.6)$$

The whole derivation is explained in detail in [9], where an interested reader finds more information. The relativistic generalisation, also known as the Liénard relation, is

$$P(t) = \frac{2}{3c} \frac{(Ze)^2}{4\pi\epsilon_0} \gamma_0^6 [\dot{\beta}_0^2 - (\beta_0 \times \dot{\beta}_0)^2] \Big|_{t_0}. \quad (2.7)$$

The Bremsstrahlung is in Fig. 2.1 represented by the smooth part of the spectrum.

2.2 Recombination

The recombination radiation is a process based on the free-bound interactions in plasma³. An electron is bounded by $(Z+1)$ -fold ionised atom, leading to a transition to a bound state of Z -fold ionised atom and emitting a photon with an energy

$$h\nu = \sqrt{m_e^2 c^4 + p_e^2 c^2} - m_e c^2 + E_Z^n, \quad (2.8)$$

where the first two terms in the right side represent the kinetic energy of the electron and the last term is the energy of the final atomic state, Z is the ion charge and n is principal quantum number. The energy of the initial electron can take value over continuum, therefore the radiation is emitted in the continuum frequency spectrum. However, the contribution of each transition must satisfy the condition $h\nu > E_Z^n$, i.e. recombination edge. That is the cause of "jumps" in the spectrum in Fig. 2.1, corresponding to different recombination stages [7].

2.3 Characteristic Radiation

The sharp lines in the spectrum in the Fig. 2.1 represent the characteristic radiation. Its origin must be sought predominantly in the inner electron shells of atoms and molecules [7]. The compulsory condition for characteristic radiation is the existence of particle with the sufficient energy, higher than the binding energy of an electron in an atom (molecule, ion) of the plasma. The incident particle ionizes or excites the bounded electron. Consequently, the vacancy creates on the position of the excited or ionized electron. An electron from higher shell⁴ falls to the vacancy. The energy difference is compensated by emitting of the photon with the energy of the shells energy difference. The situation is for better understanding depicted in Fig. 2.3 (the incident particle in figure is a cathode electron as a particle causing ionization in an X-ray tube).

³It is not necessarily in plasma, it could be in other states of matter, too.

⁴It could be the excited electron but it is not provided.

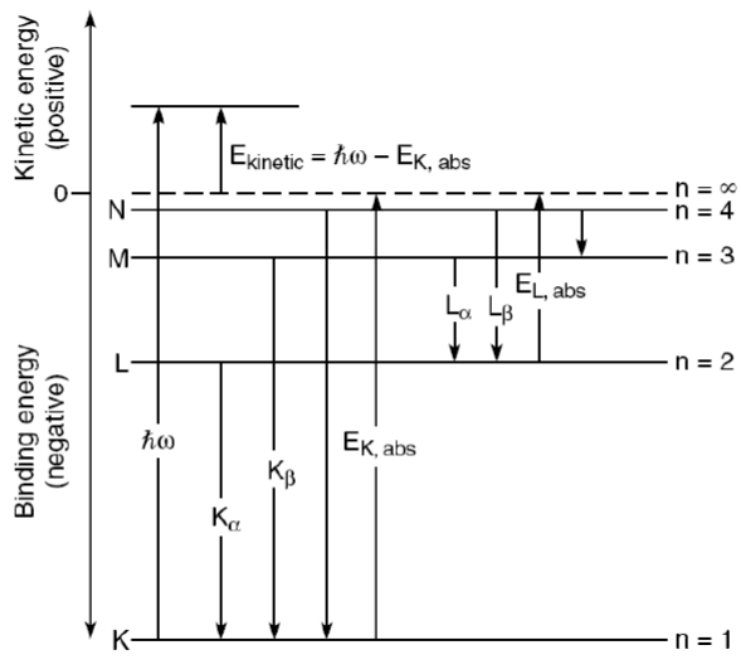


Fig. 2.3: The diagram of characteristic radiation [14].

Chapter 3

X-Ray Diagnostics and Detectors

Since the discovery of the X-rays at the end of the nineteenth century, they become a great source of diagnostics not only in the medicine but in the material sciences as well. The practical application of the X-rays required sufficient tools for describing their properties.

3.1 X-ray Detectors

The ideal information about the X-rays should contain the 3-D spatial resolution, the temporal resolution and the energy spectrum, i. e. 5 degrees of freedom. Unfortunately, typical detectors cannot provide the information about all the degrees of freedom [14]. Therefore, it is better to use multiple detectors to obtain the requested information. Some of the detectors will be introduced in the following text.

3.1.1 X-ray Film

The imaging of X-rays on X-ray films is the oldest, yet not the most frequently used method of X-ray detection. The X-ray film contains base in which crystals of a AgBr are spread. After exposing the film to X-rays, the photochemical reduction of the AgBr to a non-transparent Ag occurs. The reaction has the effect of "blackening" of the X-ray film in a certain spot. The extent of blackening is proportional to the intensity of the incident X-rays¹. The disadvantages of X-ray films are low sensitivity, resolution and disposability of the process. However, it is balanced by a low cost of the film. [15]

3.1.2 PIN Diode

The semiconductor detectors work on a principal of the inner photoelectric effect. The effect of the X-ray irradiation is a temporal increase of the conductivity of

¹The relation is valid for the intensity bellow the saturation edge of the X-ray film. [15]

the device. The PIN diode has, besides classical P and N type of semiconductor, an intrinsic part laying between the two doped semiconductors. A photo of the PIN diode and a scheme of its functioning can be found in Fig. 3.1. The intrinsic part is made of an undoped semiconductor (Si, GaAs, ...). As mentioned above, the detection ability is based on the inner photoelectric effect. The diode is reverse-biased. An incident photon of sufficiently high energy² creates an electron-hole pair. Both particles are attracted by the respective electrodes. One incident photon can create more electron-hole pairs. The result is the electric current proportional to the energy of the photon. The effort of an experimenter should lead to the one-photon events, i. e. only one photon should impact the diode in the time of the detection. If two or more photons impact the diode, the detector might consider only one photon impacting with the energy of the sum of the energies of the original photons. The PIN diodes are fast, cheap and small, which makes them popular among scientists.

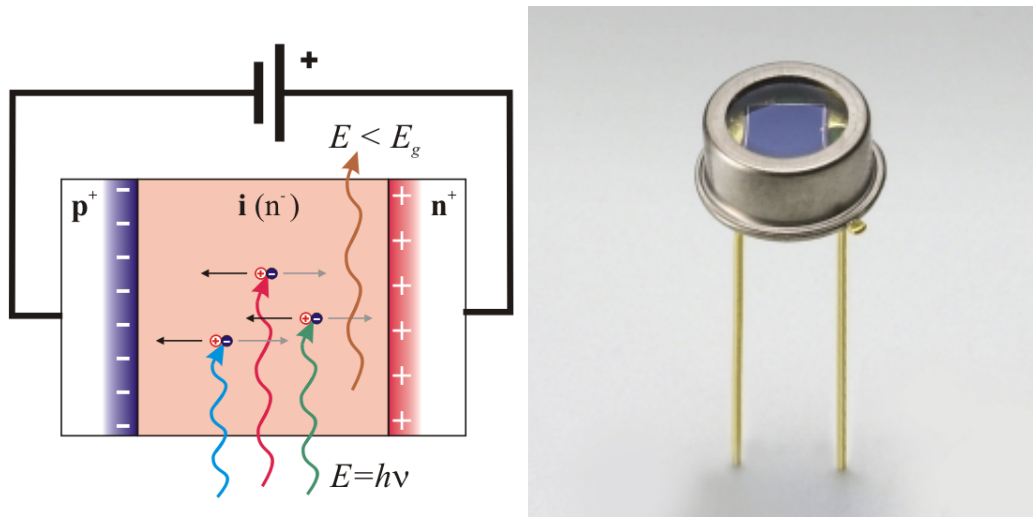


Fig. 3.1: The scheme of the PIN diode and the photo of the PIN diode. E_g is the energy for electron-hole pair generation. [16].

3.1.3 Phototube

As well as the PIN diode, the phototube works on the principle of the photoelectric effect. The difference is that in this case the photoeffect is external. A photon strikes a cathode which emits an electron. The electron is attracted to an anode and induces electric current. See the scheme of the phototube in Fig. 3.2. The phototube is filled with a gas or a vacuum. The current from the phototube is dependent on the energy and the intensity of the X-rays [17].

²For silicon intrinsic part the energy must exceed 3,62 eV at room temperature. It is the energy required for creation of electron-hole pair. [14]

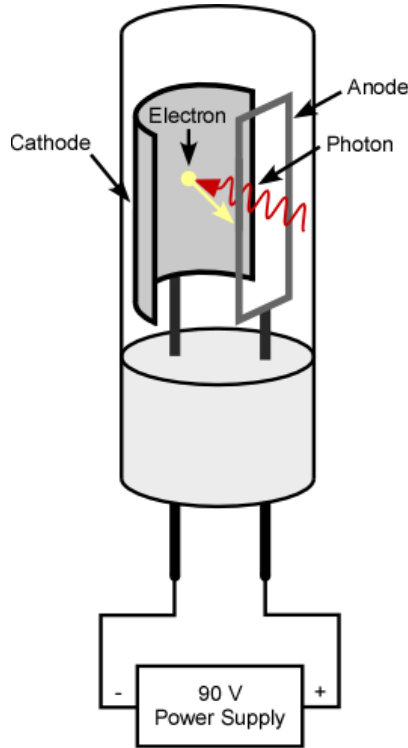


Fig. 3.2: The scheme of the phototube. [17].

3.1.4 Scintillator and Photomultiplier

The detector with the scintillator and the photomultiplier transforms X-ray photons into electric signal in two steps. The first step is held in the scintillator. It is a special material which transforms the X-ray radiation into visible or near-visible light. Luminiscent materials which show scintillation are mostly anorganic crystals (CsI, NaI, etc.) or organic materials (plastics, etc.) [14]. The physical principle of the scintillation is luminescence. An incoming X-ray photon is absorbed by the material and the energy is re-emitted in the form of the light. Then, the light enters the photomultiplier where the second part of the detection takes place. The scheme of the photomultiplier is in Fig. 3.3. The light impacts a photocathode and ionize a few photoelectrons. The photoelectrons are accelerated by the system of electrodes called dynodes and multiplied by the secondary emission. The effect is caused by the gradually increasing voltage on particle dynodes³. In the end, the electrons reach the anode. The gain of the photomultiplier is in the order of millions [14].

3.1.5 Microchannel plate

The microchannel plate (MCP) closely corresponds to the photomultiplier described above. The MCP is an array of many photomultipliers oriented in parallel with one another, see Fig. 3.4. This arrangement provides a spatial resolution to the MCP that relies on the photomultiplier channels dimensions. The dimensions are in the range

³In the typical photomultiplier, there are around ten dynodes.

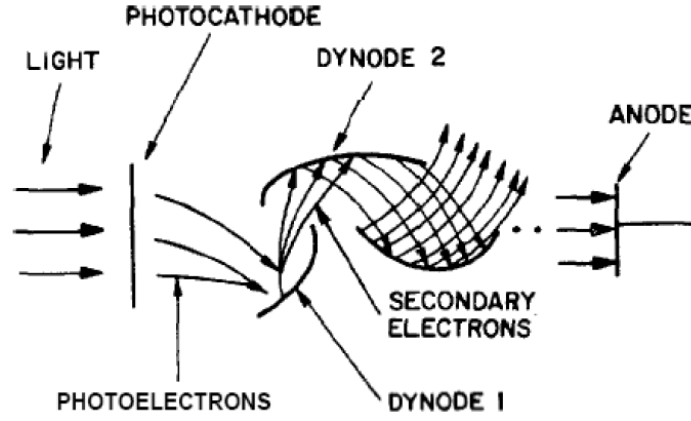


Fig. 3.3: The schematic representation of the photomultiplier tube. [14].

of 10-100 μm and have length-to-diameter ratios α between 40 and 100, [18]. The channel matrix is usually made of lead glass. The channel walls serve as a continuous dynode structure. The MCP allows electron multiplication factors of 10^4 - 10^7 , time resolution < 100 ps and spatial resolution in the order of 10 μm . The disadvantage is that the detection efficiency of X-rays is 5-15 % for the wavelength of 0.2-5 nm and falls to ~ 1 % for wavelength of 0.02-0.01 nm [18].

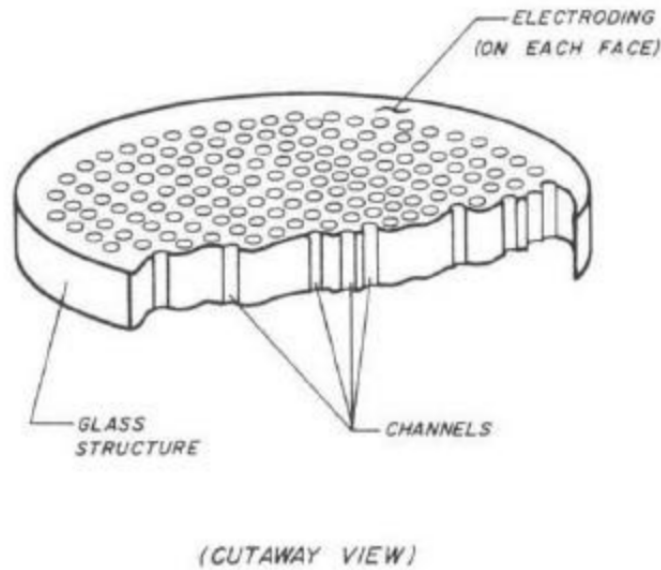


Fig. 3.4: The microchannel plate. [18].

3.1.6 Charge Coupled Device

The charged coupled device (CCD) is a small electronic device plentifully utilized in astronomy, physics, chemistry, biology and even in non-scientific fields, because it is a common part of cameras and other light-sensitive devices. In the area of X-rays, the CCD detectors have enormously improved quality and speed of the X-ray data acquisition [19]. The CCD consists of the system of the electro-optical elements that

transform X-rays to electric signal. As in the case of PIN diode, the conversion is based on inner photoelectric effect. To fully understand the following description, see Fig. 3.5. A typical CCD camera is made of three parts - a semiconductor, insulator and a system of electrodes. An X-ray photon impacts the semiconductor creating an electron-hole pair. The positively charged electrodes attract the electrons while the holes are repulsed. The contact of the electrodes and the electrons is denied by the layer of the insulator. The generated electrons move towards an oscilloscope by sequential modifying of the voltage on the electrodes. The holes are conducted to the ground. The induced electric signal is proportional to the energy of the X-ray photon. That creates a requirement of one-photon events similarly as with the PIN diode.

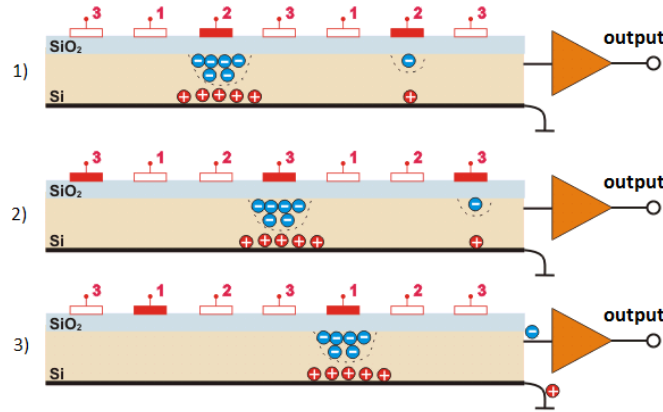


Fig. 3.5: The procedure of the reading of the X-ray information in the CCD camera. [20].

3.1.7 Streak Camera

The streak camera is very useful for the studying of the ultra short X-ray bursts created by the laser-produced plasma [21]. The physical principle is also based on the photoelectric effect. An incident X-ray photons ionize a few photoelectrons. The electrons are accelerated and deflected in the perpendicular direction by the time-variable electric field. The position of the impact on a detector⁴ is directly dependent on the voltage. By the impact position one can restore the time evolution of the incident X-rays. The schematic principle of working is in Fig. 3.6. The streak camera is distinguished by accurate time resolution in the order of 100 fs [14]. An appropriate design enables 1-D spatial and time resolution or, with using of a diffractive crystal, time and spectral resolution [14].

3.1.8 Geiger Tube

The Geiger tube⁵ is an X-ray detector utilizing the ionization ability of X-rays. The typical tube consists of the coating and the axial stick, both serving as electrodes.

⁴for example on a CCD camera

⁵also called Geiger-Müller tube

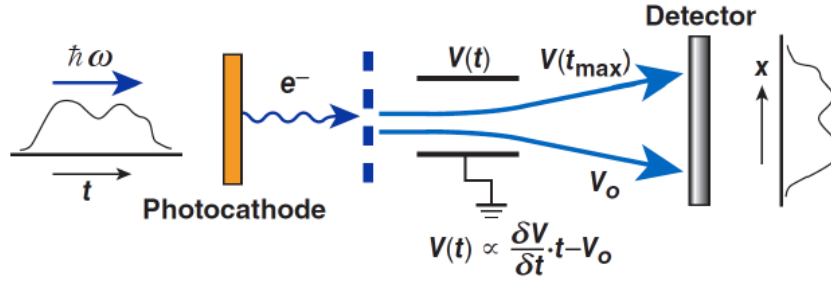


Fig. 3.6: The basic principle of the streak camera working. [14].

The tube is filled with diluted gas (e. g. neon). Between the electrodes, there is a voltage of approximately 500 V. The incoming X-ray photon causes ionization of the gas atom. The free electron is accelerated and multiplied by the mechanism of Townsend avalanche. In the tube, a discharge takes place and an electric pulse is detected [22]. The amount of pulses would be the amount of X-ray photons in the ideal Geiger detector but the real Geiger detector is not very accurate in the X-ray detection. A halogen is often added in the gas and acts as a stabilizer of the discharge [22].

3.2 X-ray Spectral Characterisation

The crucial information about X-ray radiation is its spectral distribution, i. e. the dependence of the photon number on energy⁶. The knowledge of the energy spectrum allows the application of the X-rays in the variety of fields, e. g. material sciences, astrophysics and chemistry. The common methods of the spectral determination are Bragg diffraction, Ross filters and single photon counting. One of the modern methods is a reflection off a grazing incidence mirror (ROGIM). All mentioned methods are described in more detail in the bachelor thesis [23]. In this work, the Bragg diffraction method will be reminded because it will be used in the practical part of the work.

3.2.1 Bragg Diffraction

Bragg diffraction is a useful tool for the diagnostics of X-rays or crystals owing to their interaction. The Bragg diffraction can be used for crystal identification with the known X-ray radiation or, as in our case, the X-ray properties determination with a known crystal. The interaction between the crystal and the radiation leads to the generation of the diffraction pattern if the condition in a form of the Bragg's law is fulfilled. Bragg's law was introduced by Lawrence Bragg and William Henry Bragg in 1913 [24]. It is a special case of Von Laue diffraction. Let us explain Bragg's

⁶Or on frequency ν via the relation $E = h\nu$ or wavelength λ via the relation $E = \frac{hc}{n\lambda}$, where n is the refractive index.

law in a simplified way at first for the reflection geometry and subsequently for the transmission geometry.

Reflection geometry

Assume a plane monochromatic electromagnetic wave is incident on a crystal lattice in the angle θ . The 2-D illustration of the situation is depicted in Fig. 3.7. For undergoing the constructive interference, the path difference of the reflected waves must be equal to the integer n of the wavelength λ . Mathematically expressed

$$|SQ| + |QT| = n\lambda. \quad (3.1)$$

It is clear that the relation

$$|SQ| = |QT| = d_{hkl}\sin(\theta) \quad (3.2)$$

is valid. The d_{hkl} is an interplanar distance. By substituting (3.2) to (3.1), one obtains the Bragg's condition

$$2d_{hkl}\sin(\theta) = n\lambda. \quad (3.3)$$

The relation (3.3) can be used for a spectrum acquisition. An ideal crystal⁷ with the known d_{hkl} is irradiated by the X-ray radiation with an unknown λ . The reflected radiation must follow the Bragg's condition (3.3), thus the intensity of reflected radiation changes with the variation of the incident angle θ . In an ideal case, the detected signal would be a delta function. The real signal has a shape of a rocking curve. The disadvantage could be that the method is destructive. However, there are experiments with the curved thin crystals, in which a certain part of the radiation is transmitted and the other part is reflected and diagnosed as mentioned above [26].

Transmission geometry

As in the first case, the plane monochromatic electromagnetic wave reaches a sample. The sample consists of a material with sufficient transmittance often in form of powder with randomly oriented crystals [28]. Then, the X-rays interfere behind the sample and creates a diffraction pattern (see Fig. 3.11) at the detector. The reflection geometry and the transmission geometry are illustrated in Fig. 3.8. The Bragg's law is still valid for the transmission geometry. The generalized form of the Bragg's law covering different orientation of crystal lattice is

$$\lambda = 2d_{hkl}\sin(\theta_{hkl}), \quad (3.4)$$

where θ_{hkl} is Bragg's angle for the corresponding Miller indices (h, k, l) .

⁷i. e. perfectly regular without impurities

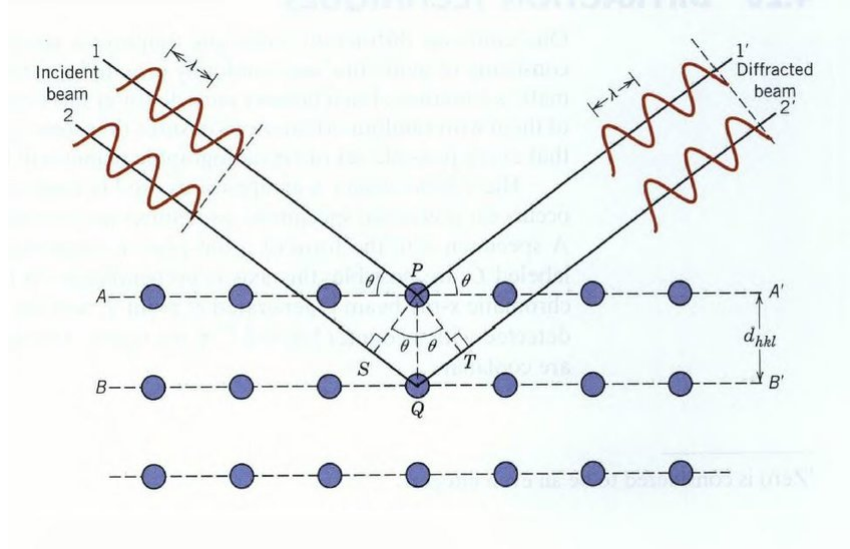


Fig. 3.7: The geometry of Bragg diffraction. [25].

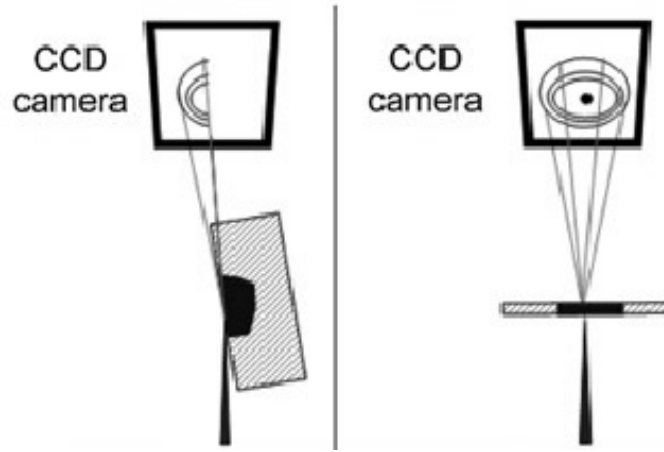


Fig. 3.8: The comparison of the reflection and transmission geometry of Bragg diffraction. [29].

X-Ray Radiation Analysis of the Data from 29. 11. 2019

The X-ray tube was used as source of X-rays for experimental Bragg diffraction analysis. The scheme of the measuring apparatus can be found in Fig. 3.10. The utilized crystal is lanthanum hexaboride. The crystal has the cubic structure with lattice parameter $a = 0.4155$ nm [27]. The distance of the detector and crystal is $l = 50$ mm. The measurement was held for 600 seconds and the resulting pattern can be found in Fig. 3.11. In Albula software, the 2D diffraction pattern was transformed in 1D dependency of the intensity on the length of the reciprocal lattice vector [$1/\text{\AA}$], see Fig. 3.9. The length of the reciprocal lattice vector q is subsequently transformed in 2θ . In the transmission geometry, it is common to state the dependency on the 2θ . Each maximum corresponds with a different crystal lattice orientation. Comparing the maxima positions with the table values of the maxima position [27] for the LaB6,

the resulting wavelength of the X-ray source is $\lambda = (0.15 \pm 1) \text{ nm}$.

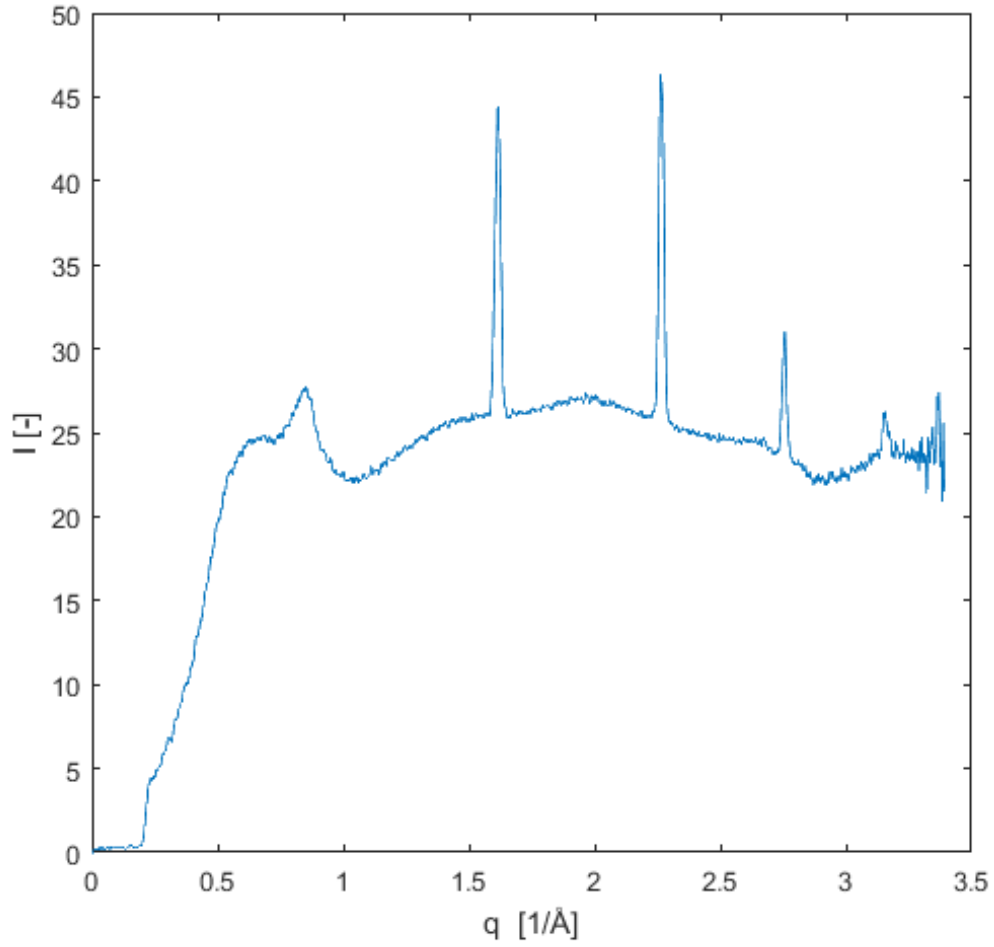


Fig. 3.9: The dependency of the intensity on the length of the reciprocal lattice vector q in $[1/\text{\AA}]$.

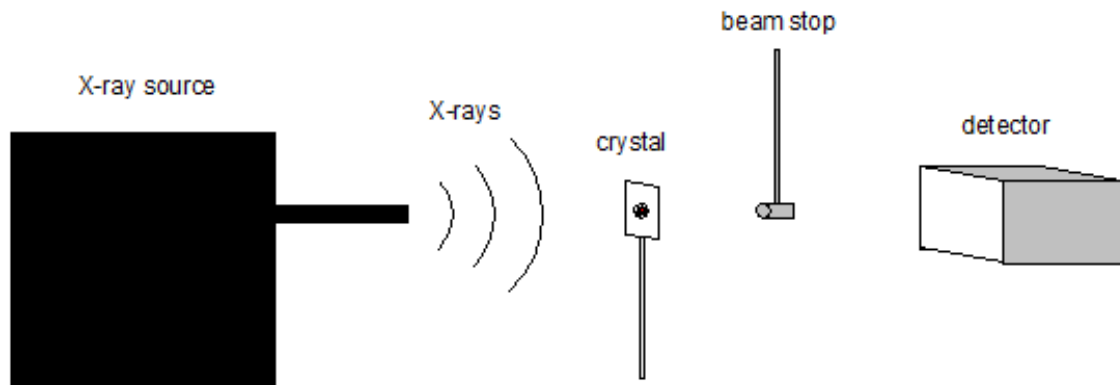


Fig. 3.10: The scheme of measuring apparatus. The beam stop is installed to reduce the intensity of radiation from the zeroth maximum.

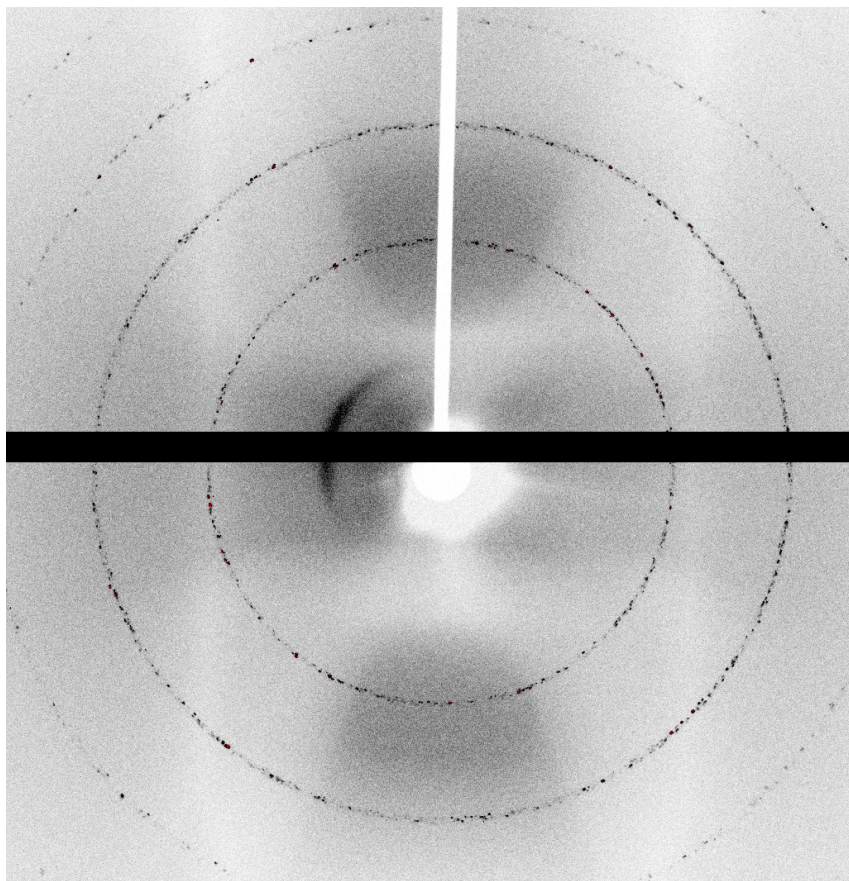


Fig. 3.11: The diffraction pattern generated by transmitting of the X-ray radiation through the lanthanum hexaboride powder.

Chapter 4

Plasma X-Ray Source

The plasma X-ray source (PXS) provides a great opportunity for creation of short X-ray pulses¹. The pulses of atomic-scale spatial resolution with ~ 100 fs temporal resolution allow studying ultrafast changes of the crystal lattice structure after optical excitation. Therefore, there appeared a high expectation of large impact on interdisciplinary research in physics, chemistry, biology and material sciences [12].

4.1 X-Ray Generation Principle

The X-rays generated in the PXS rely on femtosecond laser pulses that are focused on liquid metal (Bi-In) where they create ultrashort, high brightness X-ray pulses emitted from a microscopic spot [30]. All mechanisms of X-rays emission are described in Chapter 2.

4.2 Scheme

The whole scheme of the PXS is proceeded from a review of documentation from 2015 [30]. The construction is developed by Research Instrument Company for Extreme Light Infrastructure Beamlines Facility. The PXS is distinguished by its compactness. The brief scheme of the whole PXS device is found in Fig. 4.1. The particular parts of the PXS will be described in the following text.

4.2.1 Interior PXS layout

The PXS, its optics and beamtubes are designed for a laser beam with 76 mm diameter. For vibrational decoupling the PXS and the ELI beam line, there occur steel bellows, however, no vibration is anticipated. The bellows enter a shield wall and connect them vacuum tight to a beam transport chamber (BTC). The L-shaped

¹in order of 100 fs and below

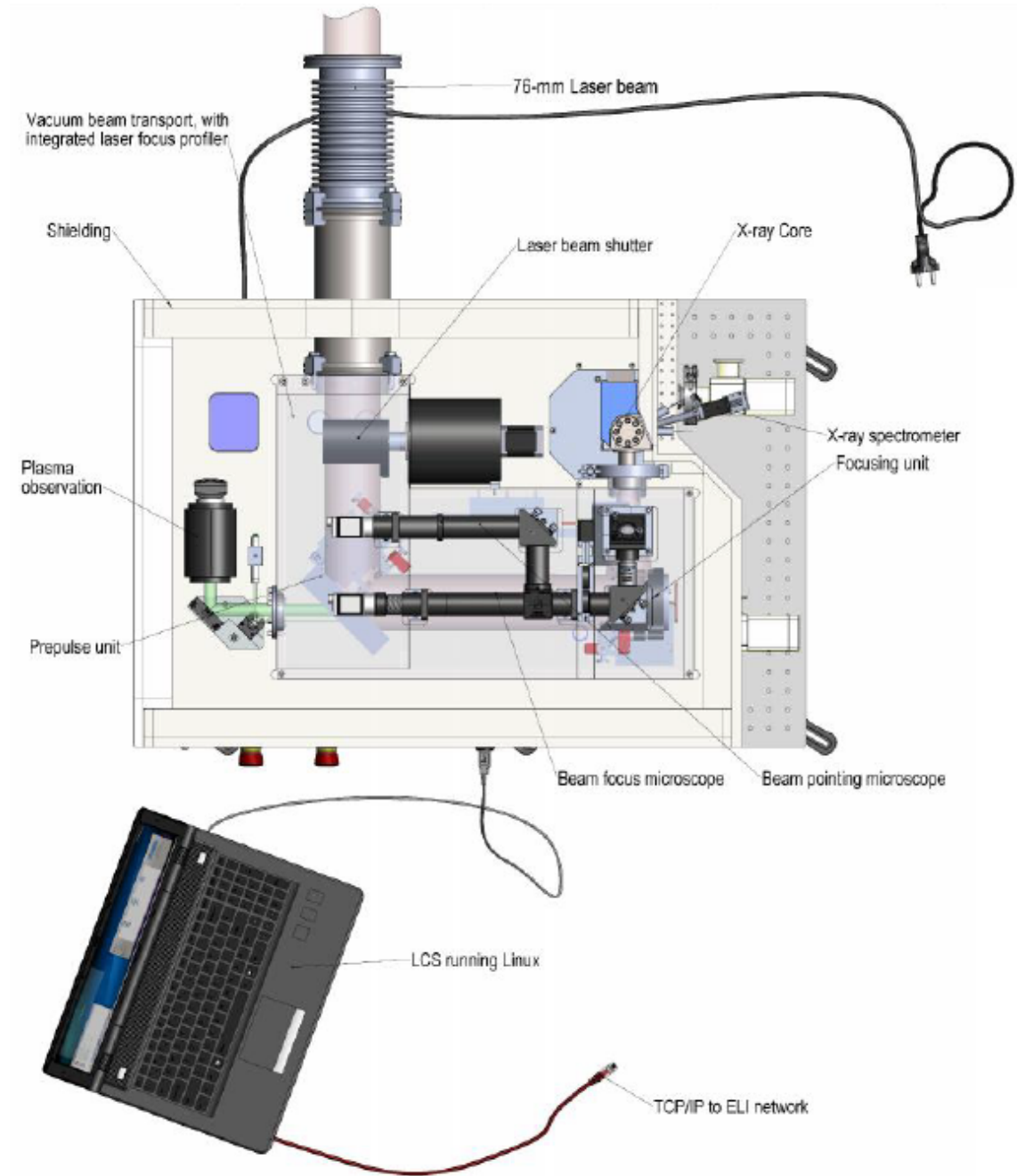


Fig. 4.1: The scheme of the PXS device [30].

BTC, semitransparently depicted in Fig. 4.1, mediates the beam transport to an X-ray core, the place where X-rays are generated. At the entrance of the BTC, there is an aluminum laser beam shutter installed. The laser beam shutter is kept opened by an actuator. In case of emergency stop or power loss, the shutter is automatically closed by gravity. The improvement of the conversion of laser light to X-rays is secured by a prepulse unit installed in front of the turning mirror. The laser beam transported through the BTC is focalized by the focusing parabola onto the liquid metal target in the X-ray core. Then, the interaction of the laser beam with plasma results in the X-ray generation. The diagnostics of the laser beam, the plasma and

the X-rays are installed in the PXS, too. The laser beam is diagnosed by a laser profiler system, the plasma is diagnosed by the plasma observation unit and the X-rays are diagnosed by the X-ray spectrometer. All three diagnostic systems will be described in detail in the separate section.

4.2.2 Beam Transport Chamber

The laser beam transport chamber has more functions than only the beam transport mediation. Also, the BTC carries the laser beam shutter (green) and laser focus profiler (orange), depicted in Fig. 4.2. The laser beam shutter consists of aluminum block mounted to axis. The block is coated black for the maximal decreasing of the backward reflectivity². A stepped motor holds the shutter open by applying the torque to the axis. The shutter is cooled by a round fin-heatsink, which is surrounded by a tube that guides a cooling air. The beam is reflected by the turning mirror, the prepulse unit and the focusing parabola. All three optical parts are mounted to the breadboard, not to the BTC housing. That is because of the providing maximum stability and the facilitation of the aligning of the laser beam.

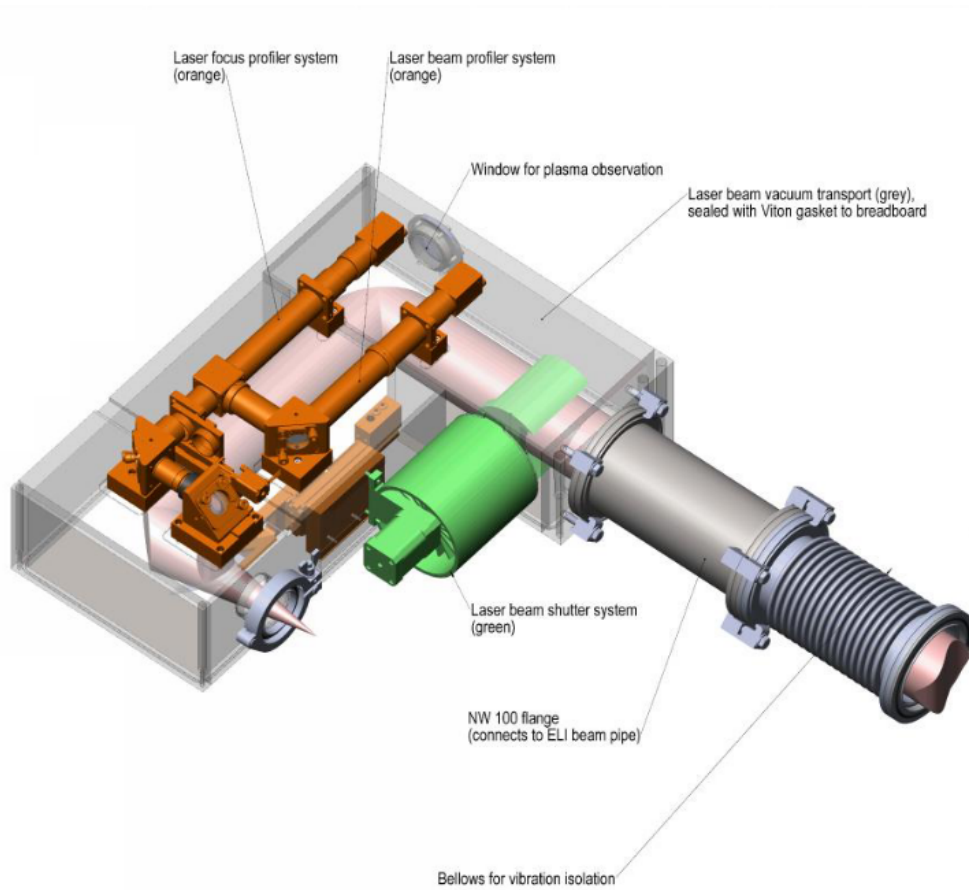


Fig. 4.2: The laser beam transport chamber [30].

²The specular reflectivity of these surfaces at 850nm wavelength is about 5%. [30]

Prepulse Unit

The laser prepulse is generated in the prepulse unit in front of the dielectric turning mirror, see Fig. 4.3. The laser prepulse is derived from the main laser pulse. The time of delay is variable (from ≤ 1 ps to ≥ 30 ps). The prepulse energy is equally variable (from 0 % to 5 % of the energy of the main pulse). The prepulse unit is installed in the PXS in order to improve conversion efficiency³. The prepulse mirror is composed of 1mm thick fused silica plate with high reflection (HR) dielectric coating centered at the laser wavelength. The HR-coated surface is facing the HR-coated surface of the main turning mirror. The distance of the main mirror and the prepulse mirror is remotely controlled by a 2-dimensional, closed-loop translation system.

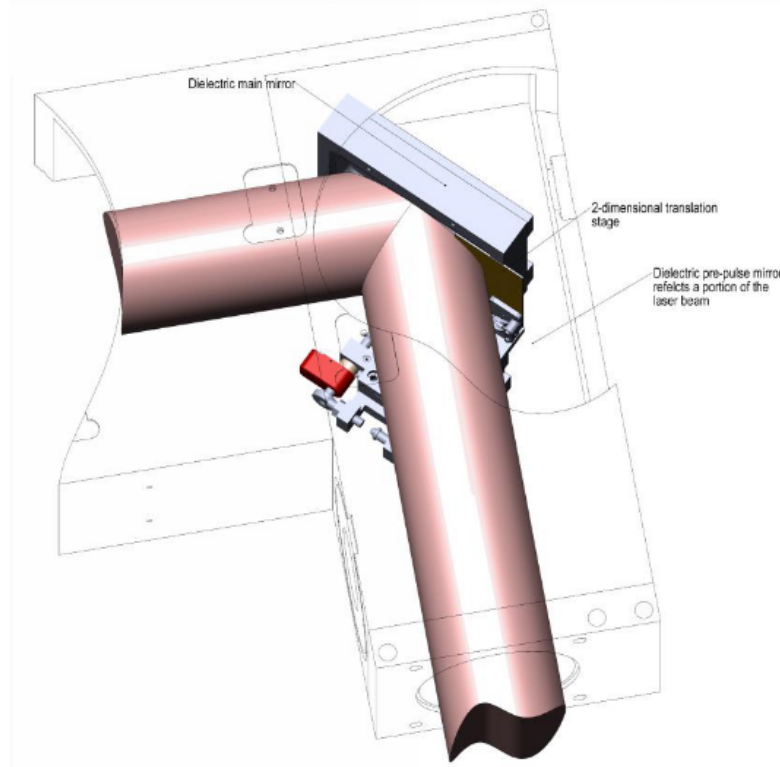


Fig. 4.3: The prepulse unit and the turning mirror [30].

Focusing Unit

The focusing unit consists of two optical parts: a focusing parabola and a vacuum window. The focusing is realized by a gold-coated parabola, located in the BTC. The reflectivity of the surface is about 98 %. The absorbed energy is removed by the heat pipe. Translations in horizontal, vertical and transversal directions are available. The horizontal and transversal translations are monitored in a closed-loop system. The vertical position is open-loop. The vacuum window is an antireflection fused silica window with 2 mm thickness and 50 mm outside curvature. The window

³The conversion efficiency may increase by order of 10 for certain types of pulses [13].

is located 76 mm from the focus. Although the vacuum window is antireflective-coated, a reflective debris from the target may change some optical properties. The debris problem will be discussed in the following section. The self-focusing length in the vacuum window is 910 m for the ELI Beamlines conditions. It results in the focus shift by $17\text{ }\mu\text{m}$, which increases the focus diameter by $3.2\text{ }\mu\text{m}$. Therefore, the intensity drops by a factor of 4. However, for the most efficient line of X-ray yield, the influence of self-focusing is negligible.

4.2.3 Plasma Observation Unit

The plasma generated by laser pulse emits very intense and broad-band light. The plasma observation unit utilizes a CCD camera for imaging plasma. It works as an inline microscope. See the scheme of the plasma observation unit in Fig. 4.4. The light generated by the plasma is colimated by the parabola. In view of the fact that the plasma light has a different wavelength than the laser light, the plasma light is transmitted through the dielectric mirror. The light is then imaged by motorized zoom lens onto a CCD camera adjusted to infinity. The plasma light intensity would over-expose the camera. Therefore, the light must be mitigated or the plasma observation unit can not be used with the full laser power. This condition is fulfilled in the case of the laser focus aligning. The plasma observation unit is also usable for the jet aligning because the debris shield heating provides enough light to image the jet.

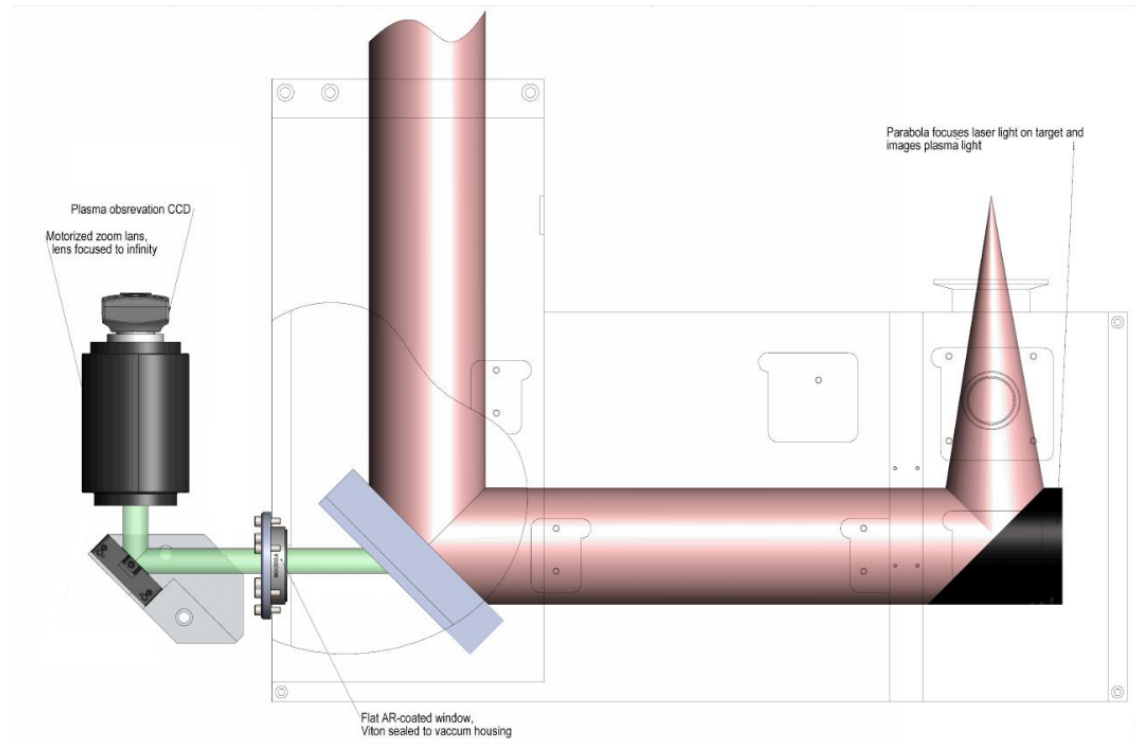


Fig. 4.4: The plasma observation unit [30], updated.

4.2.4 Laser Beam Profiler

The laser beam profiler system serves as a tool for the laser beam diagnostics. Its importance is mainly in imaging of the focus on the target. However, the focus on the target is not imaged directly. Instead, a reference focus is examined. The reference focus is identical with the original focus but it has substantially lesser intensity. The concept of the reference focus creation and the laser profiler is depicted in Fig. 4.5. The position of the laser profiler system is shown in Fig. 4.2. A beam splitter is situated between parabola and X-ray core. The beam splitter reflects 3 % of the laser power. The second beam splitter, identical to the first one, reflects the beam, so it now propagates parallelly to the top of the BTC. The identical vacuum window, as the one in the X-ray core, is installed between the splitters in the same optical distance from the focusing parabola. Thus, the optical properties of both beams will be identical, except for their intensities. The vacuum window of reference beam is coated by OD(5) neutral density metallic coating⁴. Then, the reference beam propagates through the system of lenses and is imaged by a CCD camera.

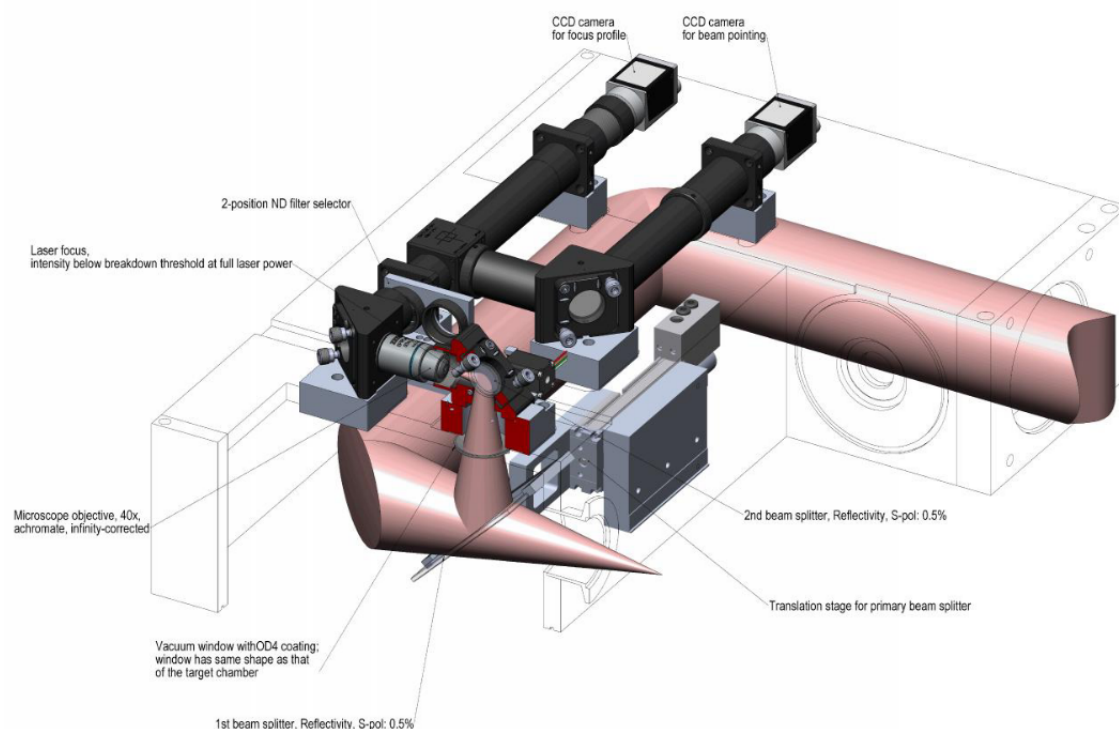


Fig. 4.5: The laser beam profiler system [30].

4.2.5 X-Ray Core

The X-ray core labels all parts of the PXS which need some maintenance. Single parts are a metal pumping system, a heat management and temperature stabilization, a

⁴The OD(X) neutral density metallic coating means, that the transition T of a filter is $T = 10^{-X}$, i.e. the light that went through has an intensity lesser by X orders.

vacuum system, and an X-ray beam and spectrometer components. In the case of the maintenance, the X-ray core is only pulled out of the PXS.

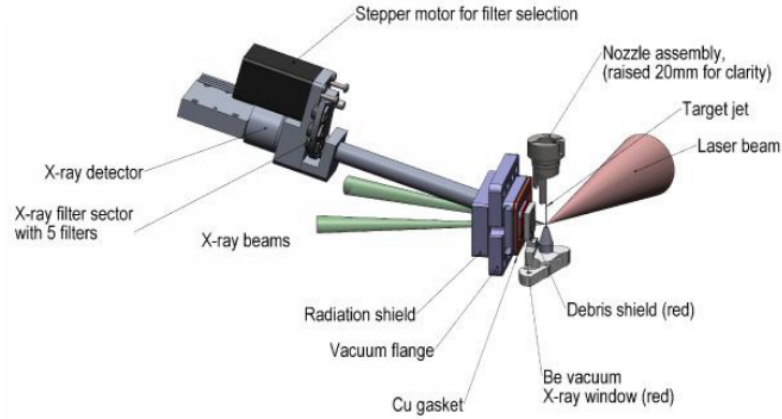


Fig. 4.6: The X-ray core [30].

Vacuum System

The proper working of the PXS requires the pressure behind the predefined threshold. The requirement is fulfilled by the vacuum system integrated in the base of the core. Due to all flanges being cooper gasket sealed, a negligible leak rate is ensured. A knife-edge system, which cuts into the copper gaskets, leads to the consequence that the system does not have to be permanently vacuum pumped. The hydrogen outgassing of the chamber walls is not problem since the chemical products of the hydrogen and target metals are chemically unstable and dissociate at room temperature. Vacuum refreshing every couple of months should be sufficient.

Target

The target is a liquid alloy consisting of 66 % indium, 34 % bismuth. The alloy melts at around 65 °C. The temperature stabilization system keeps the target and all components in contact with the target at the temperature of around 75 °C.

Target circulation system

The alloy is circulated by a magnetically-coupled gear pump. All pump parameters, e.g. the pressure of the target metal, are monitored and automatically adjusted for the optimizing target jet properties. The target jet is formed by an aluminium nozzle with dumbbell profile in order to avoid turbulences⁵. An average jet speed calculated by the theory of laminar flow through orifice is around 210 m·s⁻¹. The calculation is executed for slightly different alloy; the real jet velocity for the target

⁵Jet from a simple slit has an velocity profile from the center to the edges. This conditions might lead to problematic turbulences [30].

alloy is likely higher. The nozzle is made of aluminium. Despite, the nozzle will slowly corrode by exposing to the plasma influence. Nevertheless, the necessary replacement is required after a few thousand hours and it takes less than a few minutes.

Debris management

The problem of debris seems to be the most crucial in the PXS. The debris is produced by every laser shot and the direction of it is the direction of the laser and the X-ray windows. There were attempts of removing the debris by laser pulses themselves, which proved that the debris will be reliably cleared. The debris propagating towards the X-ray windows is reduced by various mechanisms. First of all, a debris shield is installed. The debris shield can be also heated in order to evaporate the debris. Next, the velocity of jet of approximately $200 \text{ m}\cdot\text{s}^{-1}$ reduces the angle of cone, in which the debris droplets are emitted from the target. It significantly decreases the amount of droplets hitting the internal X-ray window. Then, the experiments with electric field, used for deflecting the charged particles from the X-ray windows, are held. And finally, part of the laser pulse is reflected from the target as a result of the jet surface orientation. None of these measures are perfect but the attempts to manage the debris properly still continue.

4.2.6 X-Ray Shielding

The shielding of the PXS comprises of an approximately 45mm thick walls. The walls are mostly multi-layer and made of heavy metals. The lead in walls is used for absorbing an X-ray radiation. However, the absorbed radiation induces the secondary fluorescence of the lead atoms. Therefore, the tin is added for absorbing the fluorescence of the lead. Similarly, the fluorescence of the tin is absorbed by the steel.

4.3 Commissioning

In the June 2020 the commissioning of the PXS was held. The goals were:

- proper adjusting of the laser system and the optical system,
- testing of the debris shield functioning,
- X-ray generation.

The laser system adjusting consists of the laser power checking, the laser pulse duration checking and the optical system assembling. This part of the commissioning is rather formal but necessary in order to ensure the proper laser beam transport and the required laser beam properties. The new version of the debris shield is created of ceramics with a high-resistance wire to heat it. The heating of the debris

shield provides enough light to illuminate the jet and observe it through the plasma observation unit⁶. The result of the observation can be found in Fig. 4.7. The jet stability is the greatest for the current value $I = 4$ mA, as it is visible in Fig. 4.7c. For the different values is the jet less stable, which could affect the plasma generation.

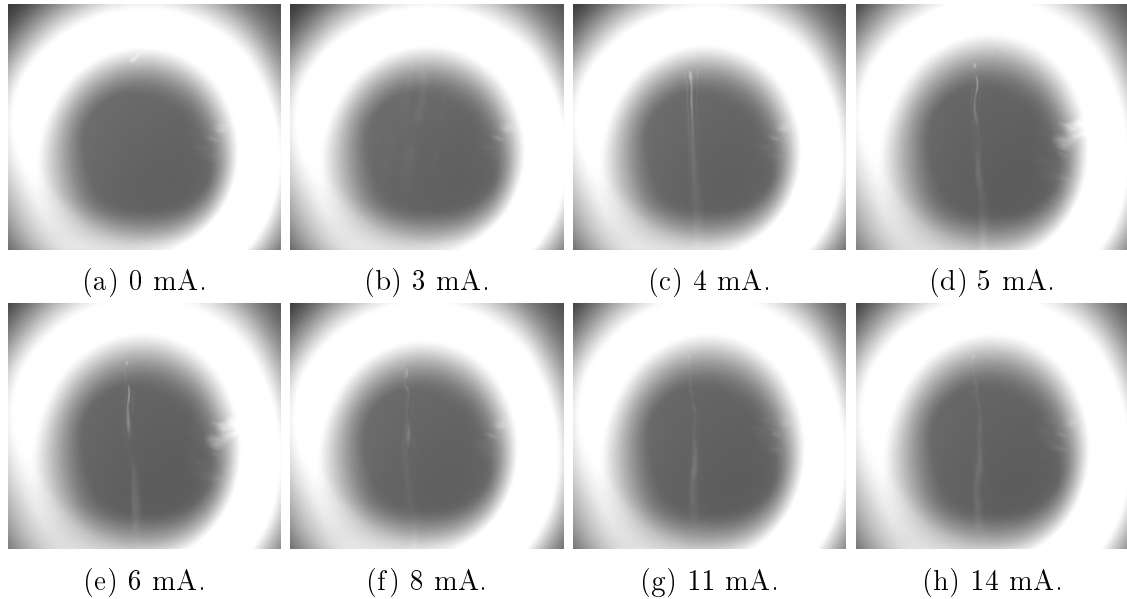


Fig. 4.7: The metal-jet adjusting. The current values at each figure represents the current in the pump.

Then, the plasma generation took place. After setting the appropriate pump current, the beam focus pointing happened. The process was firstly held in air with the laser beam hitting a shade. The reason is that the optical issues (e. g. the astigmatism) are more visible in this way. Later, the beam was directed to the X-ray core and the jet. The situation recorded by the plasma observation unit is in Fig. 4.8. The intensity of light was very high, hence a neutral density filter had been added behind the plasma observation unit. Finally, the X-ray generation was happening. There were three detectors to diagnose the incoming X-rays:

- a PIN diode⁷
- a Geiger detector
- a pinhole camera with a CCD detector.

4.3.1 Results

To successfully achieve commissioning, the photon flux must reach $2 \cdot 10^7$ photons/(shot $\cdot 4\pi$) at 10 keV. The signal detected by the PIN diode was at maximum

⁶The light is weak, therefore no mitigation of intensity is needed.

⁷The original task of the project was design and construct this detector. Nonetheless, the detector was already constructed in the research group and the task was not actual anymore.

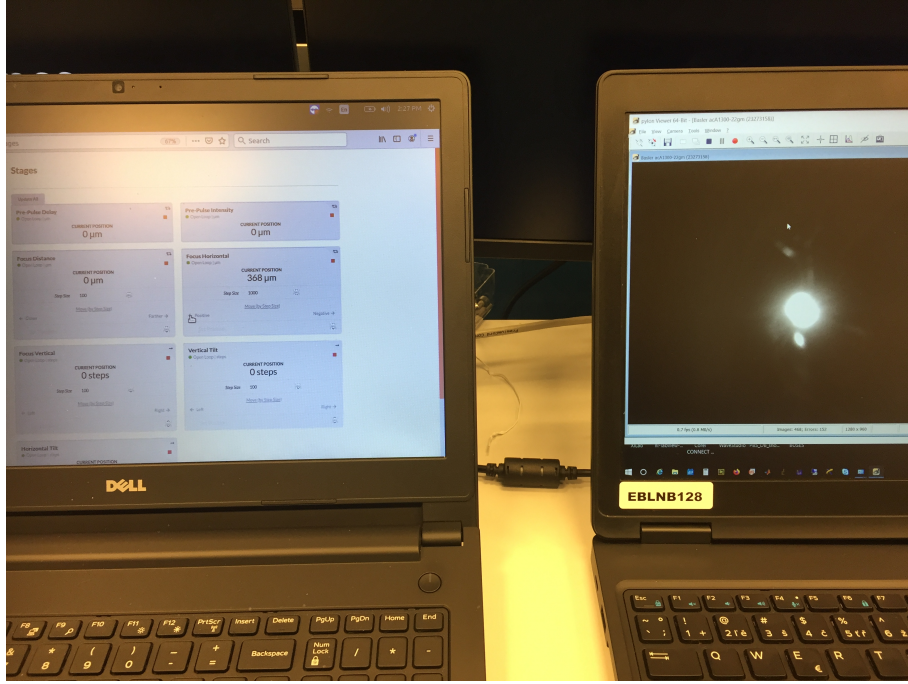


Fig. 4.8: The photo of the plasma via the plasma observation unit (right) and the optical parabola alignment panel (left).

3 mV, as seen in Fig. 4.9, which corresponds with the photon flux approximately 10 – 15 times lower than required. Furthermore, such high values was taken in the short period of time. In the longer time the values was lower. Nevertheless, the Geiger detector recorded values which imply that the PIN diode should detect tens of mV. And the data was taken in more than an hour, as can be found in Fig. 4.10. It is necessary to mention, that the Geiger detector is more sensitive for energies above 20 keV. Thus, the detection of bremsstrahlung is more probable than the detection of the Bi and In characteristic radiation. The pinhole camera with the CCD detector was used as well, but the photon flux was not high enough to detect something reasonable. The reason of the disagreement of the detectors could not be revealed before the campaign was over.

The campaign was stopped suddenly due to a debris shield crack. The crack is visible in Fig. 4.11. The reason of the cracking the debris shield ceramics is investigated. The new debris shield will be provided by Research Instrument Company.

The campaign stop allowed to discover the reason of the detector disagreement. The X-ray debris shield was fully covered by debris. The state of the X-ray debris shield before and after the campaign can be compared in Fig. 4.12. The issue explanation was then obvious. Almost all the generated X-rays, which can be detected by the PIN diode, were re-absorbed by the layer of the debris. The Geiger counter then detected the bremsstrahlung that was not re-absorbed. The resolving of the problem will require more research.

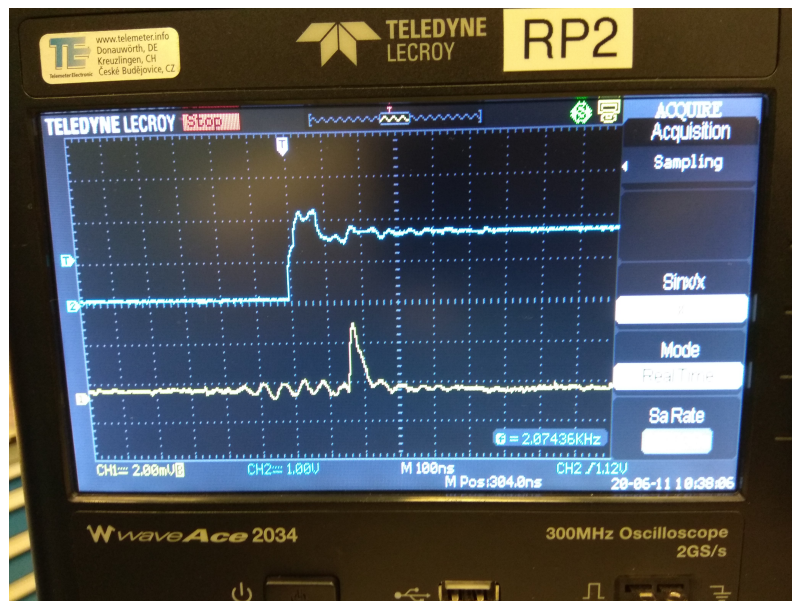


Fig. 4.9: The photo of the PIN diode data in the oscilloscope.

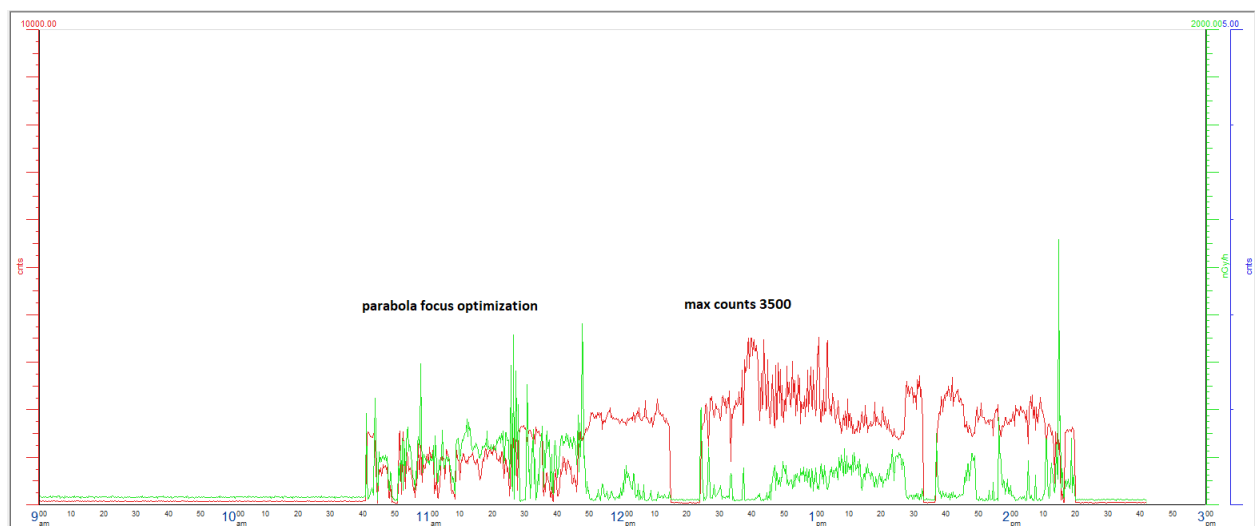


Fig. 4.10: The time dependence of counts detected by the Geiger detector.

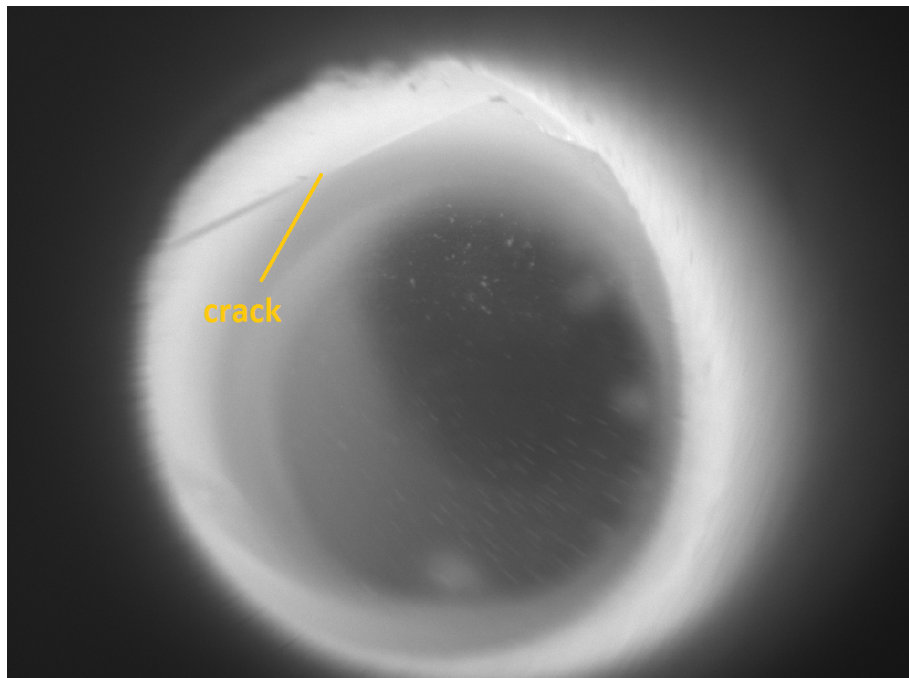
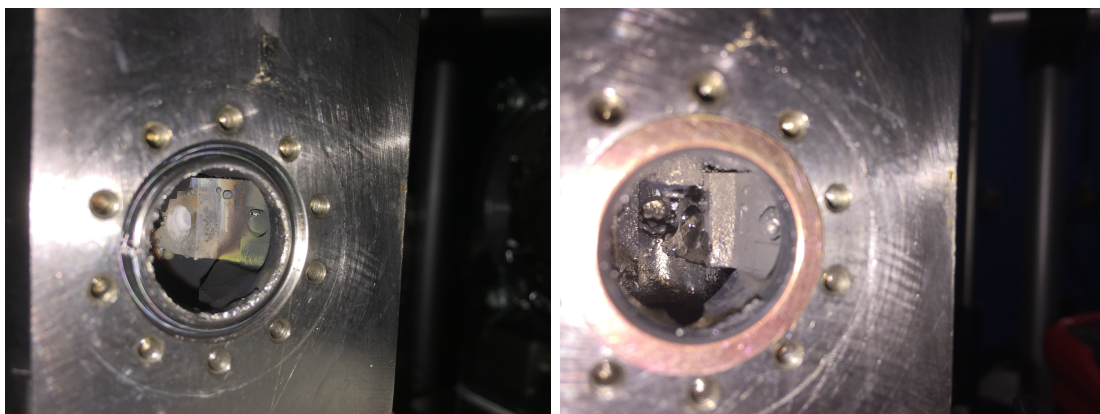


Fig. 4.11: The crack of the debris shield.



(a) before campaign

(b) after campaign

Fig. 4.12: The X-ray debris shield before and after campaign.

Summary

The aim of the project was to carry out the research of the diagnostic devices capable of acquiring the accurate and reliable information from the plasma X-ray source (PXS) in Extreme Light Infrastructure Beamlines facility in Dolní Břežany. The X-ray pulses are distinguished by short duration (~ 100 fs) and atomic-scale spatial resolution. For clarification of the PXS working, the chapters of the plasma physics elements and the X-ray generation were included. The first two chapters allowed a reader to understand the physical background of the phenomena which are important for the X-ray generation in laser plasma. The third chapter focused on X-ray detectors. The detectors are important for proper application of X-ray radiation. The chapter was divided into two parts: theoretical and practical. The theoretical part described the particular detectors, their physical principles and their feasible utilization. The practical part tried to analyse the data from the X-ray source in ELI Beamlines via the Bragg diffraction. The experiment and necessary physical basics for understanding the diagnostic process are described. The experiment took place in the *transmission geometry*. For the sake of completeness, the theory of the *reflective geometry* was included as well. The resulting wavelength $\lambda = (0.15 \pm 0.01)$ nm was corresponding to the Cu $K\alpha$ line. The result was confirmed because the source emitted the radiation of the wavelength. Finally, the fourth chapter dealt with the PXS itself. The design of the whole device as well as its particular parts were depicted in schematic figures. The chapter was based on the design review from Research Instrument Company completed with the updated information and technical solutions. The aim of the chapter was to familiarize a reader with the technical realization of the PXS and its possible difficulties. The original task concerning the detector design was obsolete since the detector was already constructed in the PXS team. The PXS is still developing and the regular commissioning are held. One of them took place in June 2020. The commissioning and its results were described in detail in the last chapter. The main outcome was that the X-ray generation was carried out successfully but the problems with debris would be a serious challenge. The project could be the starting point for the plasma X-ray source research and it could provide necessary concepts for understanding the topic.

Bibliography

- [1] M. Mo, S. Fourmaux, A. Ali, P. Lassonde, J. -C. Kieffer, and R. Fedosejevs, “Characterization of laser wakefield generated betatron X-ray radiation using grazing incidence mirror reflection”, *The European Physical Journal D*, vol. 68, no. 10, 2014.
- [2] P. Kulhánek, *Úvod do teorie plazmatu*. Praha: AGA, 2011.
- [3] D. T. Attwood, A. Sakdinawat, and L. Geniesse, *X-rays and extreme ultra-violet radiation: principles and applications*, Second edition. New York, NY: Cambridge University Press, 2016.
- [4] B. M. Smirnov, *Plasma Processes and Plasma Kinetics*. WILEY-VCH, 2008.
- [5] F. F. Chen, *Introduction to Plasma Physics and Controlled Fusion*, 3.rd ed. Los Angeles, CA, USA: Springer, Cham, 2016.
- [6] K. Boháček, *Návrh a optimalizace produkce svazků gama záření inverzním Comptonovým rozptylem femtosekundového elektronového svazku na femtosekundovém laserovém impulzu*, Diplomová práce, Praha, 2013.
- [7] D. Giulietti and L. A. Gizzi, “X-Ray Emission from Laser Produced Plasmas”, *La Rivista del Nuovo Cimento*, vol. 21, no. 1, pp. 1-104, 1998.
- [8] O. Klimo and J. Pšikal, *Základy fyziky laserového plazmatu* [lecture]. ČVUT v Praze, 2019.
- [9] I. Štoll, J. Tolar, and I. Jex, *Klasická teoretická fyzika*. Praha: Univerzita Karlova, nakladatelství Karolinum, 2017.
- [10] S. Hapugoda, “Characteristic radiation production diagram”, in *Radiopaedia.org*, 2019.
- [11] R. Almada, “What is the difference between continuous and characteristic X-Ray radiations?”, in *Quora*.
- [12] F. Zamponi, Z. Ansari, C. Korff Schmising, P. Rothhardt, N. Zhavoronkov, M. Woerner, T. Elsaesser, M. Bargheer, T. Trobitsch-Ryll, and M. Haschke, “Femtosecond hard X-ray plasma sources with a kilohertz repetition rate”, *Applied Physics A*, vol. 96, no. 1, pp. 51-58, 2009.

- [13] S. Düsterer, H. Schwoerer, W. Ziegler, D. Salzmann, and R. Sauerbrey, “Effects of a prepulse on laser-induced EUV radiation conversion efficiency”, *Applied Physics B: Lasers and Optics*, vol. 76, no. 1, pp. 17-21, Jan. 2003.
- [14] D. Klír, Diagnostika plazmatu [lecture]: *Vybrané detektory rentgenového záření*. ČVUT v Praze, 2020.
- [15] V. Vávra, RTG difraktometrie [lecture]: *Detekce RTG záření*, MUNI v Brně, 2009.
- [16] “X-ray spectroscopy with PIN photodiode”, *PhysicsOpenLab*, 2017.
- [17] “Characteristics of UV-VIS Spectrophotometric detectors”, in *Lab-training*, 2020.
- [18] J. L. Wiza, “Microchannel plate detectors”, *Nuclear Instruments and Methods*, vol. 162, no. 1-3, pp. 587-601, 1979.
- [19] S. M. Gruner, M. W. Tate, and E. F. Eikenberry, “Charge-coupled device area x-ray detectors”, *Review of Scientific Instruments*, vol. 73, no. 8, pp. 2815-2842, 2002.
- [20] J. Koutný and I. Vlk, “Postup čtení obrazové informace, Elektronika I učebnice”, in *Elektronická učebnice*, 2009.
- [21] R. Shepherd, R. Booth, D. Price, M. Bowers, D. Swan, J. Bonlie, B. Young, J. Dunn, B. White, and R. Stewart, “Ultrafast x-ray streak camera for use in ultrashort laser-produced plasma research”, *Review of Scientific Instruments*, vol. 66, no. 1, pp. 719-721, 1995.
- [22] “Jak funguje Geiger-Müllerův (GM) detektor?”, *Státní úřad radiální ochrany*, v. v. i., 2020.
- [23] M. Zhoř, “Diagnostika rentgenových svazků z laserového plazmatu”, Bakalářská práce, Praha, 2019.
- [24] “The reflection of X-rays by crystals”, *Proceedings of the Royal Society of London. Series A, Containing Papers of a Mathematical and Physical Character*, vol. 88, no. 605, pp. 428-438, 1997.
- [25] G. Bozkurt, E. B. Boşdurmaz, and I. Atasoy, “Microwave Optics-Fabry-Perot & Michelson Interferometers, Brewster’s Angle, Bragg Diffraction for PHYS374 Experiment Methods of Physics”, *ResearchGate*, March 2019.
- [26] D. Zhu, M. Cammarata, J. M. Feldkamp, D. M. Fritz, J. B. Hastings, S. Lee, H. T. Lemke, A. Robert, J. L. Turner, and Y. Feng, “A single-shot transmissive spectrometer for hard x-ray free electron lasers”, *Applied Physics Letters*, vol. 101, no. 3, Jul. 2012.
- [27] K. Persson, “Materials Data on LaB6 (SG:221) by Materials Project”, *LBNL Materials Project*, 2014.

- [28] S. Speakman, “Basics of X-Ray Powder Diffraction: Training to Become an Independent User of the X-Ray SEF at the Center for Materials Science and Engineering at MIT”, 2020, pp. 1-97.
- [29] M. Radepon, W. De Nolf, K. Janssens, G. Van der Snickt, Y. Coquinot, L. Klaassen, and M. Cotte, “The use of microscopic X-ray diffraction for the study of HgS and its degradation products corderoite, kenhsuite and calomel in historical paintings”, *ResearchGate*, pp. 1-12.
- [30] C. Rose-Petruck, *Review of Design Documentation of the PXS developed for ELI Beamlines Facility, Czech Republic*. Barrington, RI 02806-4834 U.S.A., 2015.